Beyond turbostratic disorder: Towards epitaxial alignment in $Bi_2Se_3/MoSe_2$ van-der-Waals bilayer stacks grown from amorphous elemental precursors

Fabian Göhler [1,2,3,4,*] Fabian Ganss [1,5] Aalaa Osman [1] Olav Hellwig [1,2,5]
David C. Johnson [3] and Thomas Seyller [1,2]

[1]*Institute of Physics, Chemnitz University of Technology, 09126 Chemnitz, Germany*
[2]*Center for Materials, Architectures and Integration of Nanomembranes (MAIN), 09126 Chemnitz, Germany*
[3]*Department of Chemistry, University of Oregon, Eugene, Oregon 97401, USA*
[4]*Center for Quantum Spintronics, Department of Physics, Norwegian University of Science and Technology, 7491 Trondheim, Norway*
[5]*Institute of Ion Beam Physics and Materials Research, Helmholtz-Zentrum Dresden-Rossendorf, 01328 Dresden, Germany*

(Received 30 March 2025; revised 25 June 2025; accepted 9 July 2025; published 18 July 2025)

Bottom-up synthetic approaches to synthesize stacks of individual quasi-two-dimensional materials remain a major experimental challenge. Here, we evaluate the applicability of the little-known technique of modulated elemental reactants (MER) for the synthesis of one-unit-cell-thick $Bi_2Se_3/MoSe_2$ bilayer stacks via the self-assembly of amorphous elemental Bi|Se and Mo|Se precursors. Using a two-step annealing approach, both layers can be crystallized in a single heterostructure, as evidenced by a combination of x-ray photoelectron spectroscopy, Raman spectroscopy, and x-ray diffraction. However, we observe a limited stability of the Bi_2Se_3 layer, reflected in its partial decomposition under conditions required to crystallize $MoSe_2$. The choice of substrate proves to be a crucial piece to control the thin film growth: We demonstrate the evolution of larger-scale epitaxial alignment within a heterostructure grown via MER by low-energy electron diffraction.

DOI: 10.1103/wn8y-xvyh

I. INTRODUCTION

The large-scale fabrication of quasi-two-dimensional (2D) materials using physical or chemical vapor deposition (PVD, CVD) and conversion techniques has been extensively studied in the past two decades, achieving single-crystalline growth on a wafer scale [1–4]. However, the layer-by-layer growth of vertically stacked van-der-Waals heterostructures remains a major experimental challenge [5], as growth conditions vary for each subsequent sheet in the stack and might even be incompatible with the targeted structure. The task of maneuvering a vast parameter space becomes especially arduous when more than two constituent layers are considered. For example, molecular beam epitaxy (MBE) growth of transition metal dichalcogenides (TMDC, TX_2) is usually carried out via a codeposition of the transition metal and the chalcogen, followed by annealing under high chalcogen flux above 700 °C [6,7]. On the other hand, growth of Bi_2Se thin films is generally carried out at temperatures not exceeding about 300 °C [8–11], and can be done by both MBE on crystalline substrates [12,13] or crystallization of optimized Bi|Se layers [14,15]. From this, it becomes apparent that a heterostructure combining a TMCD and Bi_2Se_3 will not be easily accessible via classical MBE approaches. Hence, the majority of research work in this field still relies on manual stacking of exfoliated flakes [16,17].

In contrast, the *modulated elemental reactants* (MER) synthesis [18,19] uses a different approach to fabricate multilayered heterostacks: In a first step, an amorphous precursor is deposited in vacuum by sequential PVD of the chosen elements. The precursor is structured in such a way that each elemental bilayer has the correct composition to yield a monolayer of the desired 2D crystal upon the subsequent self-assembly via low-temperature annealing in an inert atmosphere [20]. The layering sequence of the final product can thus be determined by controlling the nanoarchitecture of the precursor. As such, a large variety of thin films built up from metal chalcogenides (MX) and TMDC have been realized in the past [21,22]. Within these films, individual layers are aligned parallel to the growth substrate, and it was demonstrated repeatedly that the self-assembly process results in abrupt atomic interfaces [23–25]. While MER thin films generally have a thickness of a few-dozen repeating units, we were able to demonstrate in a previous report that this method can—at least in principle—also be pushed to the limit of individual 2D layers by successfully crystallizing a precursor for a single layer of semiconducting 2H–$MoSe_2$ deposited on epitaxial graphene on SiC [26]. As solid-state diffusion is limited during the annealing step in MER [23,27], the growth is instead driven by nucleation and reaction kinetics. As a result, compounds that are only kinetically stable are readily accessible [28,29], which poses a major advantage compared to more conventional synthesis approaches. However, the small diffusion lengths are also the reason that MER

*Contact author: fabian.goehler@physik.tu-chemnitz.de

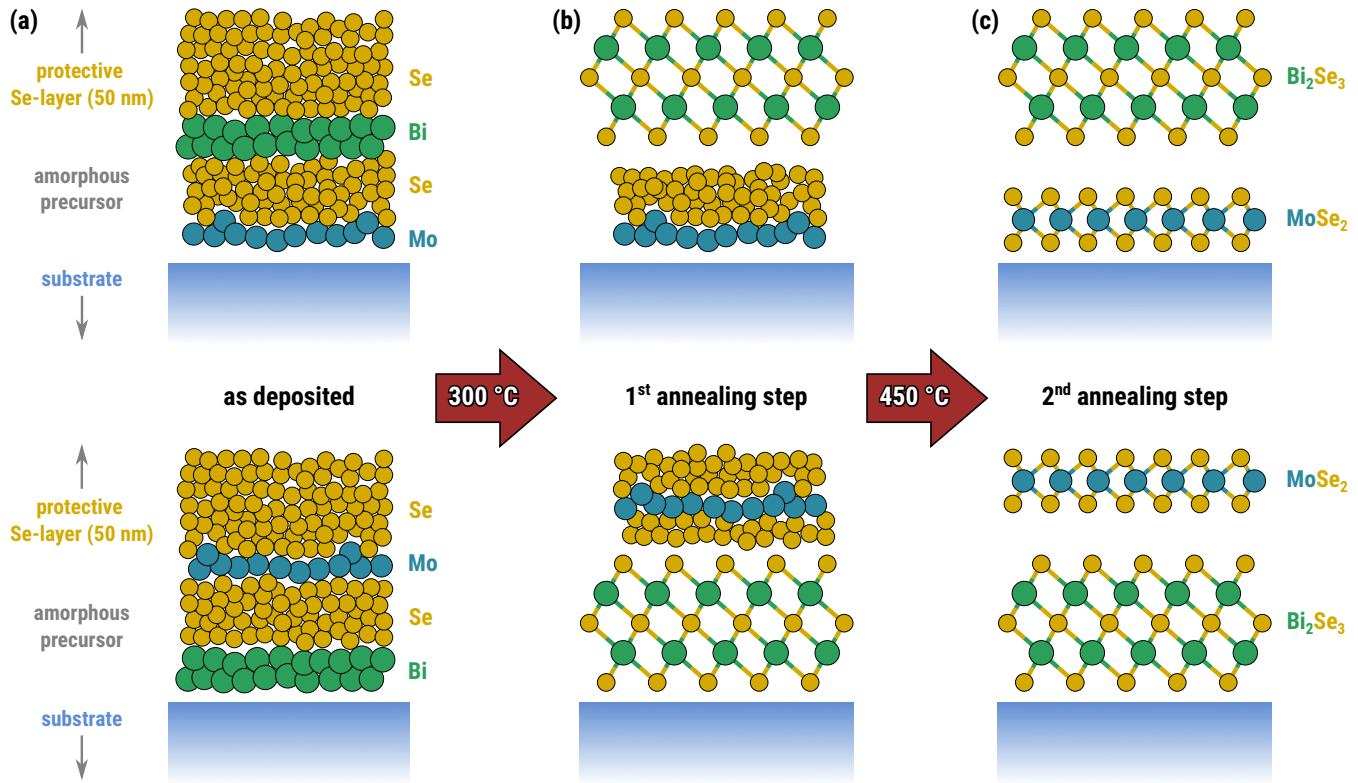

FIG. 1. Targeted growth of $Bi_2Se_3/MoSe_2$ double-layer heterostructures using MER: (a) The structure of the resulting stack is determined by the layering sequence of the elemental Bi|Se and Mo|Se bilayers in the amorphous precursors, which self-assemble into the respective crystalline layers upon annealing. Here, Bi_2Se_3 is crystallizing first (b) at lower temperatures (300 °C), followed by (c) $MoSe_2$ at 450 °C.

usually results in thin films which are polycrystalline with lateral grain sizes on the order of just a few tens of nanometers, as well as extensive rotational (turbostratic) disorder between individual layers and between grains [22,23]. This leads to ultralow lattice thermal conductivity, which can be beneficial for thermoelectric applications [25,30,31]. At the same time, it poses a severe limitation on the applicability of MER for semiconductor or spintronic devices, and—from a perspective of fundamental research—prevents access to an in-depth analysis of their electronic structure by, e.g., angle-resolved photoelectron spectroscopy (ARPES), a technique inherently reliant on sufficiently single-crystalline samples.

Nevertheless, even in such heavily disordered systems, we were able to analyze fundamental aspects such as charge distribution and charge transfer, stabilization of metastable constituent layers, and even charge-density-wave transitions by instead focusing on electronic core level and density of states (DOS) analysis using x-ray and UV-induced photoelectron spectroscopy (XPS, UPS) [32–34]. Recently, we studied the interplay of different combinations of BiSe, Bi_2Se_3, and $MoSe_2$ [35–37]. It was shown that, for example, charge transfer from BiSe into $MoSe_2$ facilitates the formation of the metallic 1T-polytype of the TMDC, which may be of interest when forming electrical contacts in devices containing 2D semiconductors [38].

These results motivated us to target the synthesis of individual bilayers of $Bi_2Se_3/MoSe_2$ and $BiSe/MoSe_2$. The vicinity to $MoSe_2$ should in principle enable the formation of both Bi_2Se_3 and the rock-salt structured BiSe: As demonstrated previously [39], elemental Bi|Se bilayers preferably convert into Bi_2Se_3 when sandwiched by a semiconductor such as PbSe or 2H–$MoSe_2$, while BiSe may form when paired with a metallic layer that can act as an electron acceptor to stabilize the structure, such as $TiSe_2$, VSe_2 or 1T–$MoSe_2$. Heterostructures consisting of interleaved few-layer $MoSe_2$ and few-layer Bi_2Se_3 have been grown *in situ* on sapphire in a layer-by-layer fashion by MBE at substrate temperatures of 340–400 °C [40]. Xenogiannopoulou *et al.* [41] demonstrated that few-layer $MoSe_2$ shows an epitaxial alignment with the underlying few-layer Bi_2Se_3 when being deposited at temperatures of 300 °C in ultrahigh vacuum (UHV). We believe that the structural disorder limitations of MER may be mitigated when performed on single-crystalline substrates. Therefore, Si(100) terminated with a native (amorphous) SiO_2 layer as well as epitaxial monolayer graphene on 6H–SiC (MLG) where chosen as growth substrates in this study to investigate the influence of the substrate crystallinity on the structural evolution of the thin-film precursor.

II. RESULTS AND DISCUSSION

A. Annealing study and characterization of thin films grown on Si(100)

The initial design of the precursors is shown schematically in Fig. 1(a): Elemental bilayers of Bi|Se and Mo|Se are deposited on the substrate at room temperature. To protect the thin films from oxidation during shipping, the precursors were capped by 50 nm of surplus Se since this is known

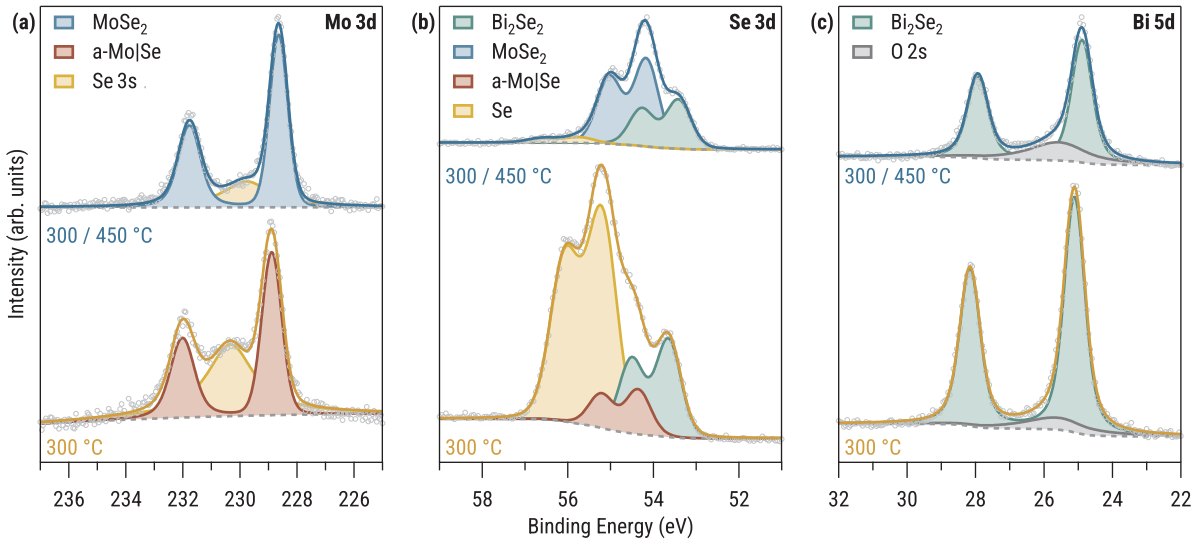

FIG. 2. XP spectra of the (a) Mo 3*d*, (b) Se 3*d*, and (c) Bi 5*d* core levels for Bi|Se|Mo|Se precursors on Si(100) after a single annealing step at 300 °C (bottom row), and after two annealing steps of 300 and 450 °C (top row). Spectra are offset for clarity.

to desorb from the surface during annealing [42]. For the targeted synthesis of $Bi_2Se_3/MoSe_2$ bilayers, precursors for both stacking configurations (Bi|Se first or Mo|Se first) were prepared. However, as will be evident later, they show only minor differences in their respective nucleation behavior.

An extended annealing study of the precursors was carried out to identify favorable conditions for the crystallization of the layers. To that end, precursors were first subjected to annealing in inert gas in a tube furnace at an Ar pressure of 900 mbar to temperatures ranging from 200 to 350 °C. However, the chemical analysis of the as-annealed films by means of XPS showed a clear Se deficit. Furthermore, the remaining Se did not bind to either Bi or Mo, as evinced by an analysis of the core-level spectra, indicating that the Se desorbs from the surface before the films are able to crystallize.

This suggests that higher pressure is required during annealing, which can be achieved by sandwiching the precursor between the substrate and an additional piece of Si or SiC wafer. This essentially traps the Se atoms and prevents a premature evaporation, as was already demonstrated in our previous attempt to crystallize a monolayer of $MoSe_2$ [26].

XPS core level spectra of such a sample after annealing at 300 °C for 30 min are shown in the bottom row of Fig. 2. The core level binding energies of the Bi 5*d* core level (which is overlapped by the O 2*s* signal stemming from the SiO_2 layer of the silicon substrate) as well as the low-binding energy component in the Se 3*d* core level [Fig. 2(b)] are consistent with the formation of Bi_2Se_3 [14]. However, most of the Se on the surface is in a state with a binding energy of 55.2 eV, consistent with unbound, elemental Se [14]. A third component is necessary to adequately fit the Se 3*d* core level, whose binding energy would be consistent with Mo-Se bonds. However, as will be evident below, this is likely not related to crystalline $MoSe_2$. Instead, we tentatively assign this component to the still amorphous Mo|Se precursor layer, and do the same in the corresponding Mo 3*d* core level.

Structural analysis of this sample was carried out using grazing incidence, in-plane XRD. The corresponding diffractogram is shown in the bottom row of Fig. 3 and features two pronounced reflections at 25.0° and 43.7°, which can be indexed to the (100) and (110) planes of Bi_2Se_3 [36]. Notably, no reflections that would be expected for $MoSe_2$ can be observed. This is consistent with the XPS results, as apparently a temperature of 300 °C is not sufficient to crystallize the Mo|Se precursor. In our previous work, successful crystallization of a monolayer $MoSe_2$ was observed after annealing to 450 °C for 60 min (although annealing was carried out inside a UHV chamber instead of a tube furnace).

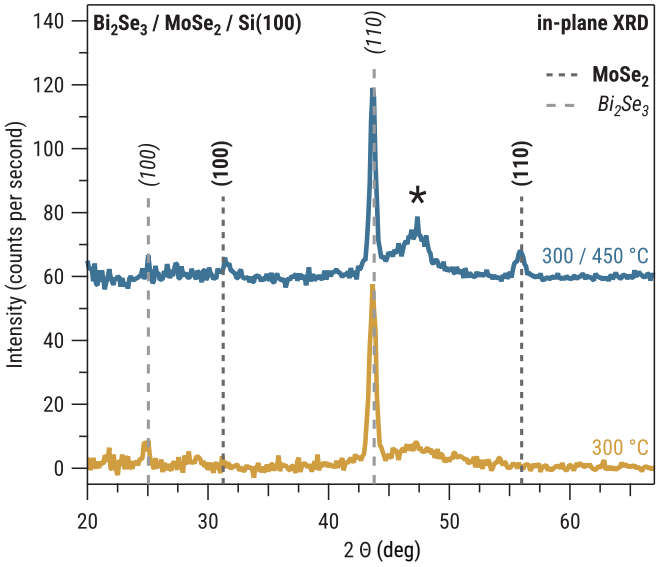

FIG. 3. Grazing incidence, in-plane XRD scans of Bi|Se|Mo|Se precursors on Si(100) after a single annealing step at 300 °C (bottom row), and after two annealing steps of 300 and 450 °C (top row). Scans are offset for clarity. The expected positions of the reflections for Bi_2Se_3 and $MoSe_2$ are indicated by dashed lines, while the peak marked with an asterisk stems from the Si substrate.

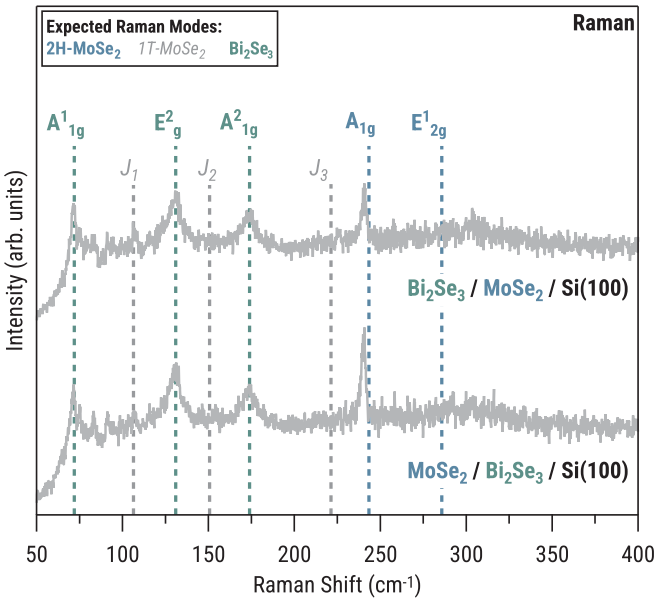

FIG. 4. Representative Raman spectra of selected $Bi_2Se_3/MoSe_2$ bilayer samples after being processed with two annealing steps. The expected positions of the Raman modes for 2H and 1T–$MoSe_2$ as well as Bi_2Se_3 are indicated by dashed lines.

A straightforward approach to facilitate the crystallization of both types of layers—Bi_2Se_3 and $MoSe_2$—would thus seem to simply increase the annealing temperature. However, in this case, higher temperatures again lead to a clear Se deficit in the annealed films. Therefore, we settled on a two-step annealing process, as depicted schematically in Figs. 1(b) and 1(c): In the first annealing step, the sample is held at a temperature of 300 °C for 30 min to crystallize the Bi_2Se_3. Subsequently, the sample temperature is raised to 450 °C and held there for another 30 min to crystallize $MoSe_2$. Afterwards, the sample is immediately removed from the hot zone of the furnace and is left to cool down in an Ar atmosphere.

XPS and in-plane XRD results of a sample processed in this manner are shown in the top rows of Figs. 2 and 3, respectively. In contrast with the sample discussed before, barely any unbound Se can be seen in the Se 3*d* core level spectrum, while the observed core level binding energies of Mo 3*d*, Se 3*d*, and Bi 5*d* are consistent with the formation of both Bi_2Se_3 and $MoSe_2$ [14,36,41]. This is confirmed by the in-plane diffraction, where now additional reflections can be observed at 31.4° and 55.9°. These can be indexed to the (100) and (110) planes of $MoSe_2$ [36]. Since all observed reflections in the diffractogram can be indexed to (*hk*0) planes, it can be concluded that the layers are aligned parallel to the surface of the substrate.

To validate the results of the in-plane diffraction, selected samples were analyzed using Raman spectroscopy after being tempered in two annealing steps. Representative results are shown in Fig. 4 for samples deposited on Si(100) substrates. A spectrum of a bare silicon wafer was subtracted from the data to account for the substrate signal. All observable Raman modes can be indexed to either 2H–$MoSe_2$ or Bi_2Se_3 [43–48]. There appears to be no contribution from the metallic 1T–$MoSe_2$ [49]. This is consistent with the XPS results and is to be expected since Bi_2Se_3 is not known to be a strong electron donor [36]. The peaks appear sharper in the sample where Bi_2Se_3 is covered by $MoSe_2$, suggesting a slightly higher degree of crystallinity and order for this stacking sequence.

In principle, Raman spectroscopy on 2D materials is sensitive to the number of layers: In $MoSe_2$, with increased thickness the A_{1g} out-of-plane vibrational mode continuously shifts to higher wave numbers for few-layer samples and shows a pronounced peak splitting for more than two layers. Tonndorf *et al.* [43] also observe a strong dependence of the relative intensity of the E^1_{2g} in-plane mode on the number of layers, but this was not reproduced unambiguously by others [44]. In our experiments, we find the A_{1g} mode of $MoSe_2$ at 240.0 cm^{-1}, which is in good agreement with literature reports on both mechanically exfoliated [43] and CVD-grown [44] monolayers on SiO_2, as well as single layers grown on epitaxial graphene via MBE or MER [26,45]. While the E^1_{2g} mode of $MoSe_2$ shows a high intensity for $MoSe_2$ on graphene [26,45], it is much less pronounced on SiO_2 substrates [43,44] and cannot be resolved in this experiment. This is likely due to the limited grain size of the thin films, discussed later. In the case of Bi_2Se_3, a significant redshift of the E^2_g mode accompanied by a blueshift of the A^1_{2g} mode has been observed by several authors when reducing the film thickness down to a few and even single layers [46–48], which some attributed to strain induced by lattice mismatch for epitaxially grown thin films [47]. Here, we find values of 71.8, 130.2, and 173.6 cm^{-1} for the A_{1g}, E^2_g, and A^1_{2g} modes of Bi_2Se_3, respectively. Even though these are closer to the reported bulk values, the general absence of strain in MER-grown thin films [50], along with the results from XPS and atomic force microscopy (discussed below), leads us to conclude that we indeed succeed in the targeted monolayer growth in the heterostructure.

B. Structure and epitaxial alignment of films grown on MLG

Precursors deposited on MLG substrates were processed in the same fashion as those on Si(100) discussed prior. Qualitatively, XPS core level spectra of the crystallized films after the two-step annealing process (see Fig. S.1 of the Supplemental Material [51]) are very similar to those on the silicon substrates shown in the top row of Fig. 2. The only notable difference is a small shift of the Mo 3*d* and Se 3*d* core levels by about 0.1–0.2 eV to higher binding energies, which could be indicative of a different interaction with the substrate. The in-plane structure of the films was investigated on selected samples via grazing incidence in-plane XRD, as shown in Fig. 5(a). Similar to the samples prepared on Si(100), all reflections can be indexed to (*hk*0) planes of Bi_2Se_3 and $MoSe_2$, which is evidence for a successful nucleation of both layer types parallel to the surface. Since graphene on SiC is a highly ordered, single-crystalline substrate, we also investigated a potential epitaxial alignment of the deposited thin films with the growth substrate. A representative low-energy electron diffraction (LEED) pattern of a $MoSe_2/Bi_2Se_3$/MLG/SiC surface is shown in Fig. 5(b). Two sets of diffraction spots with sixfold symmetry can be assigned to the graphene layer and the SiC(0001) surface, respectively. Additional superstructure spots are a consequence of the $(6\sqrt{3} \times 6\sqrt{3})R30°$

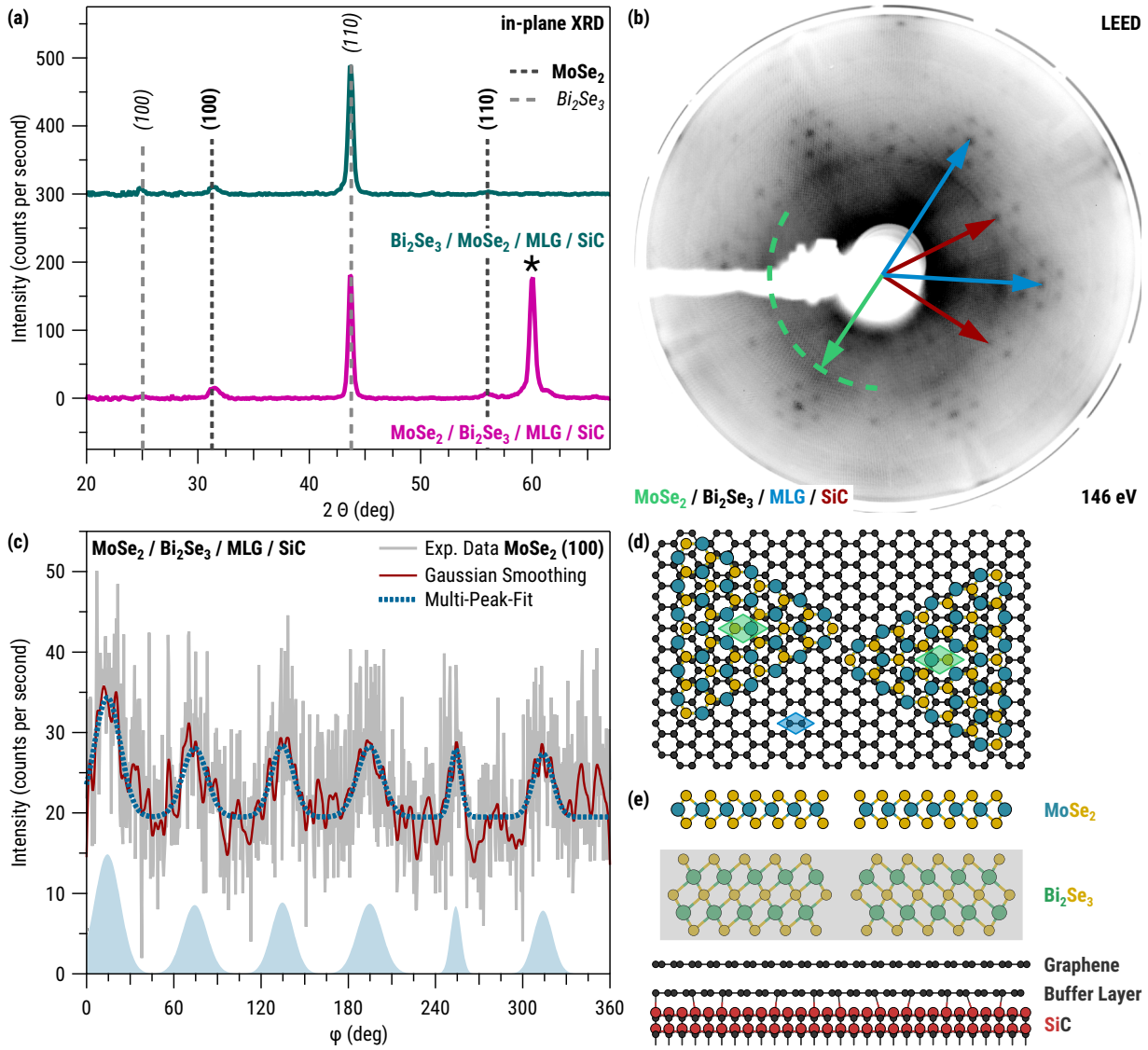

FIG. 5. Structural analysis of $Bi_2Se_3/MoSe_2$ films grown on epitaxial monolayer graphene (MLG) substrates: Representative (a) grazing incidence in-plane XRD and (b) LEED pattern of $Bi_2Se_3/MoSe_2$ samples grown on MLG after being annealed with two annealing steps at 300 and 450 °C. In-plane XRD scans are offset for clarity. The peak marked with an asterisk stems from the MLG substrate. The LEED pattern shows the expected diffraction spots of the SiC(0001) substrate and monolayer graphene, along with superstructure spots stemming from the $(6\sqrt{3} \times 6\sqrt{3})R30°$ reconstruction at the interface. Additional streaked diffraction spots along the highlighted ring are assigned to the $MoSe_2$ layer. (c) 360° φ-scan of the $MoSe_2$ (100) reflection showing six equally spaced intensity maxima separated by 60°. (d) Top view and (e) side view of the proposed structure of crystallographically aligned $MoSe_2$ domains on MLG. SiC, buffer layer, and Bi_2Se_3 have been omitted in panel (d) for clarity. In-plane unit cells of graphene and $MoSe_2$ are highlighted in blue and green, respectively. Panel (e) is viewing along the $[1\bar{1}00]$ direction of the 6H–SiC substrate. No conclusions about an epitaxial alignment of the Bi_2Se_3 layer with respect to the substrate can be drawn from the available data.

reconstruction of the buffer layer at the SiC interface [52]. Besides these diffraction spots typical for the MLG substrate, a ring-like diffraction pattern can be observed as well, which appears to show a similar lattice constant as the SiC(0001) surface unit cell (3.077 Å, [53]). As such, we can confidently assign this to the $MoSe_2$, which exhibits an in-plane lattice constant of 3.288 Å in the bulk [54]. Since the lattice constant of Bi_2Se_3 is about 25% larger than that of $MoSe_2$ [55], diffraction spots of this layer would be expected closer to the center of the screen, but cannot be resolved in the measurement. The apparent absence of a diffraction pattern for Bi_2Se_3 is unfortunate but not unexpected: Even in fully crystallized, thicker MER-grown thin films, LEED patterns are at best very diffuse due to small lateral grain sizes of the crystallites [26,34,56]. Remarkably, the $MoSe_2$ diffraction ring shows pronounced intensity maxima in the direction of the reciprocal lattice vectors of the graphene layer, indicating that the thin films are at least in part epitaxially aligned. Here, we want to emphasize that, qualitatively, the same diffraction patterns emerge independently of the layering sequence of $MoSe_2$ and Bi_2Se_3, as shown in Fig. S.2 of the Supplemental Material [51]. The alignment can also be verified by an in-plane XRD φ-scan, as demonstrated in Fig. 5(c): Here, the intensity of the $MoSe_2$ (100) reflection is recorded while

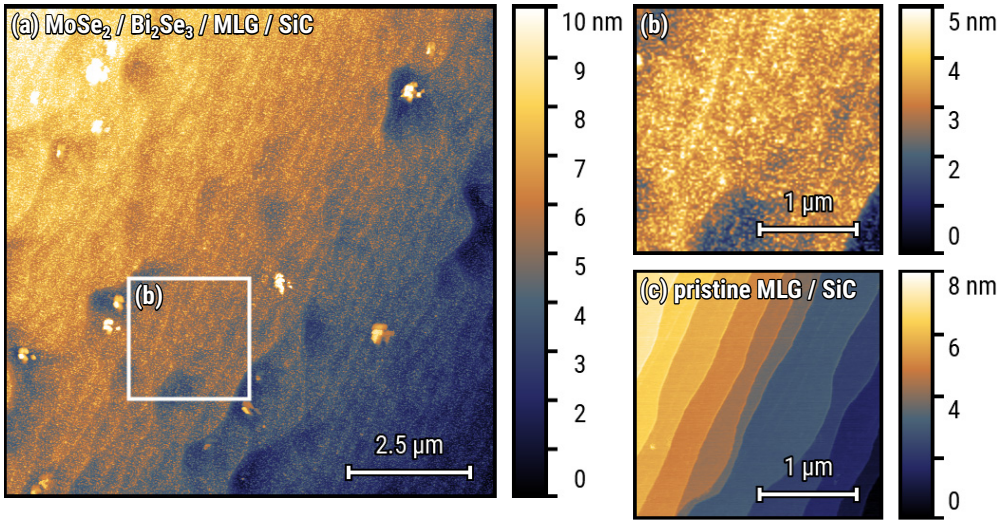

FIG. 6. (a) Large-scale atomic force microscopy (AFM) image of a crystallized $MoSe_2/Bi_2Se_3$/MLG/SiC sample. The underlying flat terraces are due to the stepped structure of the SiC surface terminated by MLG. The image was adjusted so that terraces appear at equal height. The larger bright protrusions are likely due to contaminants on the surface, as AFM was carried out *ex situ*. Panel (b) shows an enlarged view of the region highlighted in panel (a), in comparison with a (c) pristine MLG surface. The bilayer films crystallize in small grains, homogeneously covering the otherwise flat terraces of the MLG substrate.

rotating the sample a full 360° around the surface normal. A multiple peak fit to the data shows six equally spaced maxima separated by 60°, in excellent agreement with the information from LEED. The fit was performed after first applying a Gaussian smoothing to the data to reduce numerical artifacts. An analogous analysis of the Bi_2Se_3 (110) reflection across multiple processed samples for both stacking sequences generally revealed no clear evidence for or against a similar alignment. This can likely be attributed in part to the short lateral coherence lengths—caused by the small in-plane crystallite sizes discussed below—which result in a broadening or smearing out of intensity maxima in diffraction experiments [57,58]. As shown in Fig. S.3 of the Supplemental Material [51], in rare cases, the Bi_2Se_3 (110) φ-scan of individual samples appears to show very weak intensity maxima, which might hint at the possibility that this layer could develop at least a partial alignment with the substrate as well.

The emergence of six intensity maxima in LEED and XRD implies that two mirrored domains of $MoSe_2$ must coexist on the sample surface, as indicated in Fig. 5(d), because—in contrast with graphene—TMDC exhibit only a threefold rotational symmetry. A comprehensive structural model of the crystallized thin films is shown in Figs. 5(d) and 5(e). Although the available data do not allow any conclusions to be drawn as to whether the Bi_2Se_3 layers are also epitaxially aligned with the substrate, these results are nevertheless in stark contrast with all previous experiments [23,26,34], where no preferred crystalline orientation within the film plane was observed at all. Generally, thin films prepared via MER are known to be polycrystalline with extensive rotational disorder between layers owing to their nucleation-driven growth process [22], with only very few exceptions showing some form of longer-range order [59]. Our results suggest that choosing a sufficiently commensurate single-crystalline substrate may facilitate the growth of highly ordered thin films from elemental precursors. As discussed in the introduction, this would mitigate one of the main limitations of MER.

Atomic force microscopy (AFM) is a viable tool to analyze the lateral structure and topography of surfaces and thin films. A representative topography image of a $MoSe_2/Bi_2Se_3$/MLG sample is shown in Figs. 6(a) and 6(b). The results are very similar to those reported previously on MER-grown single-layer $MoSe_2$: A well-known arrangement of parallel terraces originates from the SiC substrate steps, which are covered by monolayer graphene [60]. As seen in Fig. 6(c), pristine MLG substrates show atomically flat terraces. After the MER process, they are densely covered by a grainy structure, which indicates that the $MoSe_2/Bi_2Se_3$ bilayers grow in a multitude of small grains, not dissimilar to thicker MER thin films. The enlarged view in Fig. 6(b) shows that most crystallites are too small to resolve their structure, but some individual grains show a pronounced triangular shape with an edge length on the order of 100 nm. Triangular flakes are a common occurrence in the growth of 2D TMDC when the stoichiometry is slightly off the ideal 1 : 2 ratio [61]. Height profile analysis of selected grains (Fig. S.4 of the Supplemental Material [51]) is consistent with the formation of stacked $MoSe_2/Bi_2Se_3$ bilayers, considering their known respective monolayer thicknesses of approximately 6.5 Å for $MoSe_2$ and 9.55 Å for Bi_2Se_3 in the bulk [47,62]. In contrast, other regions show apparent heights corresponding to only one of the two layers. This is indicative of either an incomplete formation or a partial decomposition of the desired heterostructure, as we discuss in detail below.

C. Chemical composition and stability of bilayer thin films

Next, we want to discuss the chemical composition of the thin films after finalization of the two-step annealing process. In XPS, the measured peak area I_{expt} of a core level is proportional to the respective atomic density on the surface.

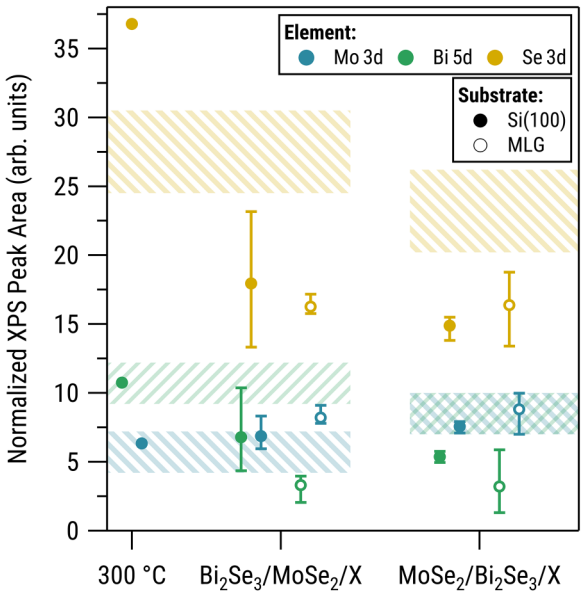

FIG. 7. Normalized XPS core-level peak areas for the three elements Mo, Bi, and Se in the thin films after two annealing steps of 300 and 450 °C. The peak intensities of the sample annealed to only 300 °C are given as a reference. Filled and open symbols correspond to samples prepared on Si(100) or MLG, respectively. Shaded areas indicate the expected peak area for a complete coverage with Bi_2Se_3 and $MoSe_2$.

In order to compare signals from different core levels, the measured peak areas have to be normalized by the respective photoionization cross section σ_i (based on calculations by Scofield [63]), inelastic mean free path λ (after Tanuma, Powell & Penn [64]), as well as the instrument-specific analyzer transmission function T:

$$I_{\text{norm}} = \frac{I_{\text{expt}}}{\sigma_i \lambda_{MoSe_2}(E_{\text{kin}}) T(E_{\text{kin}})}. \quad (1)$$

The normalized peak areas after Eq. (1) are plotted in Fig. 7 for the two different stacking sequences and depending on the growth substrate [Si(100) or MLG]. Here, data points correspond to average values and error bars represent the observed spread in experimental data over multiple samples prepared independently. Shaded areas indicate the expected intensity of the core level peaks which are calculated from the size of the in-plane unit cells of the two constituent layers, assuming an idealized two-layer model. Due to the extreme surface sensitivity of XPS, the expected peak intensity depends on the layering sequence of the heterostructure, as the signal from the bottom layer is attenuated by inelastic scattering in the topmost layer. Since our AFM measurements suggest that the as-crystallized bilayer films show inhomogeneous coverage with interspersed monolayer regions, deviations from this idealized model can provide insights into the formation and stability of the heterostructure. The values obtained on the sample processed in only one annealing step at 300 °C, which still features excess unbound Se and no crystallized $MoSe_2$ as discussed in the beginning, are given as a reference as well.

From Fig. 7, two issues become apparent: (1) all films annealed via the two-step process show a pronounced Se deficit compared to the expectation; and (2) while the Mo concentration on the surface appears relatively constant, the films do show a pronounced loss of Bi, which can amount to more than 50% of the Bi initially deposited. This is surprising, since Bi_2Se_3 is expected to be reasonably stable once crystallized [65–67], even though there has been some debate over the stability of Bi_2Se_3 surfaces in the past [68,69]. For example, photo-emission experiments carried out by Edmonds *et al.* on cleaved single crystals of Bi_2Se_3 [70] show a decomposition of the top-most Bi_2Se_3 quintuple layer upon brief exposure to air, which forms an elemental Bi bilayer on the surface. However, in the experiments presented here, XRD and Raman measurements were carried out *ex situ* over a span of hours or days, and the presence of Bi_2Se_3 could still be witnessed independently by XRD, Raman, and XPS regardless. Most importantly, our XPS spectra (such as Fig. 2) do not show any signs of elemental Bi or bismuth oxides as would be expected if the crystallized Bi_2Se_3 decomposes.

It appears reasonable to assume that the second annealing step destabilizes the Bi_2Se_3. To test this hypothesis, the sample deposited on Si(100) and annealed to only 300 °C discussed in the beginning—which verifiably consisted of crystallized Bi_2Se_3—was subjected to a second process at elevated temperature in the same conditions known to crystallize $MoSe_2$ [26]. For a stable configuration, one would assume that the remaining Mo and Se atoms bind together to form $MoSe_2$ while leaving the Bi_2Se_3 layer intact. However, the opposite is observed in experiment, as can be seen in the top row of Fig. 8: After the second process, the Mo 3*d* and Se 3*d* core levels are indeed consistent with the presence of $MoSe_2$, but the Bi_2Se_3 has vanished completely. Not even trace amounts of Bi can be observed in the Bi 5*d* core level spectrum, and the corresponding low-binding energy component in the Se 3*d* core level is gone as well. We suspect that the nanocrystalline nature of our MER thin films observed in AFM (Fig. 6) may be a major reason for this behavior because 2D nanocrystals of Bi_2Se_3 and Bi_2Te_3 were found to decompose at temperatures ranging from 280 to 500 °C via the sublimation of chalcogen atoms starting on the $\{01\bar{1}0\}$ planes [71]. In our system, the small grain size of the as-crystallized Bi_2Se_3 layer offers a high ratio of available edge sites, which in turn likely lower its stability.

Finally, we want to briefly report on our attempts targeting $BiSe/MoSe_2$ bilayer samples. As shown for example by Choffel *et al.* [37], the targeted synthesis of either Bi_2Se_3 or the metastable, rocksalt-structured BiSe in MER delicately depends on the composition of the precursor. Samples were processed in similar fashion as the precursors for $Bi_2Se_3/MoSe_2$ discussed before. Since the chemical states of the Bi and Se atoms are similar for both structural variants, they cannot be distinguished by XPS [36]. BiSe does however show a pronounced (110) diffraction peak in in-plane XRD, located at either 29° for a square in-plane unit cell or 28.0°–28.5° for a rectangular one [36]. As can be seen in Fig. S.5 in the Supplemental Material [51], a weak signal can be observed in this region on samples prepared on both Si(100) and MLG. However, it appears that the hexagonal polytype of Bi_2Se_3 is predominantly formed, with only minor contributions of BiSe. In LEED [Fig. S.2 (c)], no diffraction

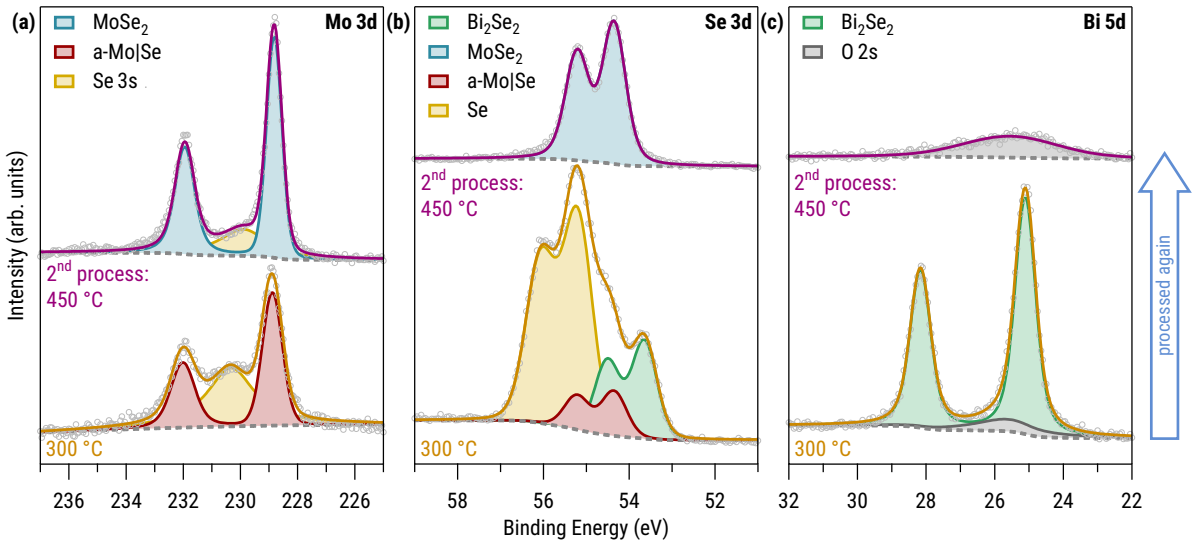

FIG. 8. XP spectra of the (a) Mo 3*d*, (b) Se 3*d* and (c) Bi 5*d* core levels of a $Bi_2Se_3/MoSe_2$ sample on Si(100) after an initial single annealing step at 300 °C (bottom row), and after being processed again at 450 °C (top row). Spectra are offset for clarity.

spots corresponding to either BiSe, Bi_2Se_3, or $MoSe_2$ can be observed, indicating a higher amount of structural disorder compared with $Bi_2Se_3/MoSe_2$. We suggest that the stabilization of single-layer BiSe outside of thicker MER thin films or misfit layer compounds may require a single-crystalline substrate with a cubic surface unit cell as an epitaxial template, coupled with a charge-accepting layer such as 1T–$MoSe_2$ or other metallic 2D material.

III. CONCLUSION

In this study, we demonstrated that the modulated elemental reactants (MER) synthesis approach—usually reserved for the creation of heterostacks of quasi-two-dimensional thin films with a thickness on the order of a few tens to hundreds of nanometers—can be successfully applied to grow bilayer stacks of Bi_2Se_3 and 2H–$MoSe_2$ with only a single repeating unit normal to the substrate surface. Albeit the stabilization of the complete Bi_2Se_3 layer proves difficult in the presence of $MoSe_2$, both layers can be synthesized via a two-step annealing process in a controlled environment. This is confirmed experimentally by a combination of spectroscopy (XPS, Raman) and diffraction (grazing-incidence in-plane XRD). In contrast to all previous reports on MER-grown thin films—which are characterized by extensive rotational disorder—low-energy electron diffraction (LEED) experiments performed on crystallized $Bi_2Se_3/MoSe_2$ bilayer samples unequivocally demonstrate a partial epitaxial alignment of the $MoSe_2$ layer with respect to the substrate when the growth is carried out on single-crystalline graphene on SiC. This opens up an avenue to form truly single-crystalline MER thin films via the simple choice of an appropriate substrate, which should enable both their use in device applications as well as a more in-depth analysis of their electronic structure [e.g., by means of angle-resolved photoelectron spectroscopy (ARPES)]. This is of fundamental interest for layer combinations hosting correlated electron phenomena such as charge-density waves or nontrivial band topology.

IV. EXPERIMENTAL DETAILS

Epitaxial graphene substrates (MLG) were prepared on SiC wafers purchased from *NovaSiC* and *Cree* using the Ar-assisted and polymer-assisted sublimation growth on SiC described in detail elsewhere [1,60,72]. Elemental Bi|Se and Mo|Se bilayers with calibrated thicknesses to form one monolayer of Bi_2Se_3, BiSe, or $MoSe_2$ were deposited onto Si(100) substrates with native SiO_2 and MLG substrates in a custom-built deposition chamber. To prevent oxidation and contamination of the as-deposited precursors, an additional elemental Se layer with a thickness of 50 nm was deposited on top.

Annealing studies as discussed in the main manuscript were carried out in a *Carbolite CTF 12/65/550* tube furnace at an Ar pressure of 900 mbar.

Initial analysis of as-grown films was carried out after brief exposure to air using x-ray photoelectron spectroscopy (XPS) performed in a UHV system equipped with a monochromatic *SPECS Focus 500* Al Kα x-ray source and a *SPECS Phoibos 150* hemispherical analyzer with 9-channeltron detector. For low-energy electron diffraction (LEED), a *SPECS ErLEED 150* was available. Prior to LEED experiments, samples were carefully and briefly degassed at temperatures below 300 °C, which is the lower limit of the pyrometer available for temperature monitoring. The base pressure of the UHV system was better than 3×10^{-10} mbar.

Selected samples were further analyzed ex-situ with Raman spectroscopy on a *LabRam HR800* with an excitation wavelength of 514.7 nm and a 2400 grooves per mm grating, atomic force microscopy (AFM) on a *Park Systems XE100*, and X-ray diffraction (XRD) on a *Rigaku SmartLab 9 kW* with *HyPix-3000* detector using CuKα radiation ($\lambda = 1.5419$ Å). For all XRD 2θ scans shown in the manuscript, a polynomial

background was subtracted from the data to remove intensity caused by inelastic scattering and scattering in air.

ACKNOWLEDGMENTS

F. Göhler acknowledges funding by the German Academic Exchange Service (DAAD) by means of the Federal Ministry of Education and Research (BMBF) within the project "International Promovieren an der TU Chemnitz (InProTUC)." The authors would like to thank Constance Schmidt for assistance with Raman measurements.

F. Göhler, D.C.J., and T.S. conceived the project. Sample preparation and experiments were carried out by F. Göhler, F. Ganss, and A.O., F. Göhler carried out the data analysis, made the figures, and wrote the manuscript with significant input from all authors.

DATA AVAILABILITY

The data that support the findings of this article are not publicly available. The data are available from the authors upon reasonable request.

[1] K. V. Emtsev, A. Bostwick, K. Horn, J. Jobst, G. L. Kellogg, L. Ley, J. L. McChesney, T. Ohta, S. A. Reshanov, J. Röhrl, E. Rotenberg, A. K. Schmid, D. Waldmann, H. B. Weber, and T. Seyller, Towards wafer-size graphene layers by atmospheric pressure graphitization of silicon carbide, Nat. Mater. **8**, 203 (2009).

[2] C. Muratore, A. A. Voevodin, and N. R. Glavin, Physical vapor deposition of 2D van der Waals materials: A review, Thin Solid Films **688**, 137500 (2019).

[3] T. Kang, T. W. Tang, B. Pan, H. Liu, K. Zhang, and Z. Luo, Strategies for controlled growth of transition metal dichalcogenides by chemical vapor deposition for integrated electronics, ACS Mater. Au **2**, 665 (2022).

[4] J. Li, S. Wang, L. Li, Z. Wei, Q. Wang, H. Sun, J. Tian, Y. Guo, J. Liu, H. Yu, N. Li, G. Long, X. Bai, W. Yang, R. Yang, D. Shi, and G. Zhang, Chemical vapor deposition of 4-inch wafer Scale Monolayer $MoSe_2$, Small Science **2**, 2200062 (2022).

[5] J. Li, J. Liang, X. Yang, X. Li, B. Zhao, B. Li, and X. Duan, Controllable preparation of 2D vertical van der Waals heterostructures and superlattices for functional applications, Small **18**, 2107059 (2022).

[6] D. Fu, X. Zhao, Y.-Y. Zhang, L. Li, H. Xu, A.-R. Jang, S. I. Yoon, P. Song, S. M. Poh, T. Ren, Z. Ding, W. Fu, T. J. Shin, H. S. Shin, S. T. Pantelides, W. Zhou, and K. P. Loh, Molecular beam epitaxy of highly crystalline monolayer molybdenum disulfide on hexagonal boron nitride, J. Am. Chem. Soc. **139**, 9392 (2017).

[7] W. Pacuski, M. Grzeszczyk, K. Nogajewski, A. Bogucki, K. Oreszczuk, J. Kucharek, K. E. Połczyńska, B. Seredyński, A. Rodek, R. Bożek, T. Taniguchi, K. Watanabe, S. Kret, J. Sadowski, T. Kazimierczuk, M. Potemski, and P. Kossacki, Narrow excitonic lines and large-scale homogeneity of transition-metal dichalcogenide monolayers grown by molecular beam epitaxy on hexagonal boron nitride, Nano Lett. **20**, 3058 (2020).

[8] J. E. Brom, L. Weiss, T. H. Choudhury, and J. M. Redwing, Hybrid physical–chemical vapor deposition of Bi_2Se_3 films, J. Cryst. Growth **452**, 230 (2016).

[9] P. Tabor, C. Keenan, S. Urazhdin, and D. Lederman, Molecular beam epitaxy and characterization of thin Bi_2Se_3 films on Al_2O_3(110), Appl. Phys. Lett. **99**, 013111 (2011).

[10] L. He, F. Xiu, Y. Wang, A. V. Fedorov, G. Huang, X. Kou, M. Lang, W. P. Beyermann, J. Zou, and K. L. Wang, Epitaxial growth of Bi_2Se_3 topological insulator thin films on Si(111), J. Appl. Phys. **109**, 103702 (2011).

[11] X. F. Kou, L. He, F. X. Xiu, M. R. Lang, Z. M. Liao, Y. Wang, A. V. Fedorov, X. X. Yu, J. S. Tang, G. Huang, X. W. Jiang, J. F. Zhu, J. Zou, and K. L. Wang, Epitaxial growth of high mobility Bi_2Se_3 thin films on CdS, Appl. Phys. Lett. **98**, 242102 (2011).

[12] G. Zhang, H. Qin, J. Teng, J. Guo, Q. Guo, X. Dai, Z. Fang, and K. Wu, Quintuple-layer epitaxy of thin films of topological insulator Bi_2Se_3, Appl. Phys. Lett. **95**, 053114 (2009).

[13] A. Richardella, D. M. Zhang, J. S. Lee, A. Koser, D. W. Rench, A. L. Yeats, B. B. Buckley, D. D. Awschalom, and N. Samarth, Coherent heteroepitaxy of Bi_2Se_3 on GaAs (111)B, Appl. Phys. Lett. **97**, 262104 (2010).

[14] T.-H. Kim, J. H. Baeck, H. Choi, K.-H. Jeong, M.-H. Cho, B. C. Kim, and K. T. Jeong, Phase transformation of alternately layered Bi/Se structures to well-ordered single crystalline Bi_2Se_3 structures by a self-organized ordering process, J. Phys. Chem. C **116**, 3737 (2012).

[15] J. Chae, S.-H. Kang, Y.-K. Kwon, and M.-H. Cho, Suppression of the hybridization of surface states and transport property in ultrathin Bi_2Se_3/graphene heterostructure, Appl. Sci. Converg. Technol. **28**, 207 (2019).

[16] H. Guo, Z. Hu, Z. Liu, and J. Tian, Stacking of 2D materials, Adv. Funct. Mater. **31**, 2007810 (2020).

[17] A. Castellanos-Gomez, X. Duan, Z. Fei, H. R. Gutierrez, Y. Huang, X. Huang, J. Quereda, Q. Qian, E. Sutter, and P. Sutter, Van der Waals heterostructures, Nat. Rev. Methods Primers **2**, 58 (2022).

[18] D. C. Johnson, Controlled synthesis of new compounds using modulated elemental reactants, Curr. Opin. Solid State Mater. Sci. **3**, 159 (1998).

[19] M. Noh, C. D. Johnson, M. D. Hornbostel, J. Thiel, and D. C. Johnson, Control of reaction pathway and the nanostructure of final products through the design of modulated elemental reactants, Chem. Mater. **8**, 1625 (1996).

[20] D. M. Hamann, D. Bardgett, D. L. M. Cordova, L. A. Maynard, E. C. Hadland, A. C. Lygo, S. R. Wood, M. Esters, and D. C. Johnson, Sub-monolayer accuracy in determining the number of atoms per unit area in ultrathin films using X-ray fluorescence, Chem. Mater. **30**, 6209 (2018).

[21] A. M. Miller and D. C. Johnson, Challenges in synthesis of heterostructures, J. Mater. Chem. C **10**, 6546 (2022).

[22] M. Beekman, C. L. Heideman, and D. C. Johnson, Ferecrystals: Non-epitaxial layered intergrowths, Semicond. Sci. Technol. **29**, 064012 (2014).

[23] D. L. M. Cordova and D. C. Johnson, Synthesis of metastable inorganic solids with extended structures, ChemPhysChem **21**, 1345 (2020).

[24] M. Esters, M. B. Alemayehu, Z. Jones, N. T. Nguyen, M. D. Anderson, C. Grosse, S. F. Fischer, and D. C. Johnson, Synthesis of inorganic structural isomers by diffusion-constrained self-assembly of designed precursors: A novel type of isomerism, Angew. Chem. Int. Ed. **54**, 1130 (2015).

[25] E. C. Hadland, H. Jang, N. Wolff, R. Fischer, A. C. Lygo, G. Mitchson, D. Li, L. Kienle, D. G. Cahill, and D. C. Johnson, Ultralow thermal conductivity of turbostratically disordered $MoSe_2$ ultra-thin films and implications for heterostructures, Nanotechnology **30**, 285401 (2019).

[26] F. Göhler, E. C. Hadland, C. Schmidt, D. R. T. Zahn, F. Speck, D. C. Johnson, and T. Seyller, Growth of nanocrystalline $MoSe_2$ monolayers on epitaxial graphene from amorphous precursors, Phy. Status Solidi B **256**, 1800283 (2019).

[27] F. Harvel, M. Lemon, R. N. Gannon, D. Bardgett, M. Humphrey, and D. C. Johnson, Investigation of the Pb–Fe–Se ternary system and the synthesis of a ternary $Pb_{1-x}Fe_x$ Se phase, Chem. Mater. **34**, 6339 (2022).

[28] A. C. Lygo, D. M. Hamann, D. B. Moore, D. R. Merrill, J. Ditto, M. Esters, J. Orlowicz, S. R. Wood, and D. C. Johnson, Kinetically controlled formation and decomposition of metastable $[(BiSe)_{1+\delta}]_m[TiSe_2]_m$ compounds, J. Am. Chem. Soc. **140**, 3385 (2018).

[29] M. Lemon, F. G. Harvel, R. N. Gannon, P. Lu, S. P. Rudin, and D. C. Johnson, Targeted synthesis of predicted metastable compounds using modulated elemental reactants, J. Vac. Sci. Technol. A **41**, 022203 (2023).

[30] C. Chiritescu, D. G. Cahill, N. Nguyen, D. C. Johnson, A. Bodapati, P. Keblinski, and P. Zschack, Ultralow thermal conductivity in disordered, layered WSe_2 crystals, Science **315**, 351 (2007).

[31] E. Hadland, H. Jang, M. Falmbigl, R. Fischer, D. L. Medlin, D. G. Cahill, and D. C. Johnson, Synthesis, characterization, and ultralow thermal conductivity of a lattice-mismatched $SnSe_2(MoSe_2)_{1.32}$ heterostructure, Chem. Mater. **31**, 5699 (2019).

[32] F. Göhler, G. Mitchson, M. B. Alemayehu, F. Speck, M. Wanke, D. C. Johnson, and T. Seyller, Charge transfer in $(PbSe)_{1+\delta}(NbSe_2)_2$ and $(SnSe)_{1+\delta}(NbSe_2)_2$ ferecrystals investigated by photoelectron spectroscopy, J. Phys.: Condens. Matter **30**, 055001 (2018).

[33] F. Göhler, D. M. Hamann, N. Rösch, S. Wolff, J. T. Logan, R. Fischer, F. Speck, D. C. Johnson, and T. Seyller, Electronic structure of designed $[(SnSe)_{1+\delta}]_m[TiSe_2]_2$ heterostructure thin films with tunable layering sequence, J. Mater. Res. **34**, 1965 (2019).

[34] F. Göhler, S. Ramasubramanian, S. K. Rajak, N. Rösch, A. Schütze, S. Wolff, D. L. M. Cordova, D. C. Johnson, and T. Seyller, Modulation doping and charge density wave transition in layered PbSe-VSe_2 ferecrystal heterostructures, Nanoscale **14**, 10143 (2022).

[35] E. C. Hadland, F. Göhler, G. Mitchson, S. S. Fender, C. Schmidt, D. R. T. Zahn, T. Seyller, and D. C. Johnson, Synthesis and properties of $(BiSe)_{0.97}MoSe_2$: A heterostructure containing both 2H–$MoSe_2$ and 1T–$MoSe_2$, Chem. Mater. **31**, 5824 (2019).

[36] F. Göhler, M. A. Choffel, C. Schmidt, D. R. T. Zahn, D. C. Johnson, and T. Seyller, Influence of nanoarchitectures on interlayer interactions in layered Bi–Mo–Se heterostructures, J. Phys. Chem. C **125**, 9469 (2021).

[37] M. A. Choffel, R. N. Gannon, F. Göhler, A. M. Miller, D. L. Medlin, T. Seyller, and D. C. Johnson, Synthesis and electrical properties of a new compound $(BiSe)_{0.97}(Bi_2Se_3)_{1.26}(BiSe)_{0.97}(MoSe_2)$ containing metallic 1T-$MoSe_2$, Chem. Mater. **33**, 6403 (2021).

[38] R. Kappera, D. Voiry, S. E. Yalcin, B. Branch, G. Gupta, A. D. Mohite, and M. Chhowalla, Phase-engineered low-resistance contacts for ultrathin MoS_2 transistors, Nat. Mater. **13**, 1128 (2014).

[39] M. A. Choffel, T. M. Kam, and D. C. Johnson, Substituent effects in the synthesis of heterostructures, Inorg. Chem. **60**, 9598 (2021).

[40] S. Vishwanath, X. Liu, S. Rouvimov, L. Basile, N. Lu, A. Azcatl, K. Magno, R. M. Wallace, M. Kim, J.-C. Idrobo, J. K. Furdyna, D. Jena, and H. G. Xing, Controllable growth of layered selenide and telluride heterostructures and superlattices using molecular beam epitaxy, J. Mater. Res. **31**, 900 (2016).

[41] E. Xenogiannopoulou, P. Tsipas, K. E. Aretouli, D. Tsoutsou, S. A. Giamini, C. Bazioti, G. P. Dimitrakopulos, P. Komninou, S. Brems, C. Huyghebaert, I. P. Radu, and A. Dimoulas, High-quality, large-area $MoSe_2$ and $MoSe_2/Bi_2Se_3$ heterostructures on AlN(0001)/Si(111) substrates by molecular beam epitaxy, Nanoscale **7**, 7896 (2015).

[42] D. L. M. Cordova, T. M. Kam, R. N. Gannon, P. Lu, and D. C. Johnson, Controlling the self-assembly of new metastable tin vanadium selenides using composition and nanoarchitecture of precursors, J. Am. Chem. Soc. **142**, 13145 (2020).

[43] P. Tonndorf, R. Schmidt, P. Böttger, X. Zhang, J. Börner, A. Liebig, M. Albrecht, C. Kloc, O. Gordan, D. R. T. Zahn, S. M. de Vasconcellos, and R. Bratschitsch, Photoluminescence emission and Raman response of monolayer MoS_2, $MoSe_2$, and WSe_2, Opt. Express **21**, 4908 (2013).

[44] J. C. Shaw, H. Zhou, Y. Chen, N. O. Weiss, Y. Liu, Y. Huang, and X. Duan, Chemical vapor deposition growth of monolayer $MoSe_2$ nanosheets, Nano Res. **7**, 511 (2014).

[45] M. M. Ugeda, A. J. Bradley, S.-F. Shi, F. H. da Jornada, Y. Zhang, D. Y. Qiu, W. Ruan, S.-K. Mo, Z. Hussain, Z.-X. Shen, F. Wang, S. G. Louie, and M. F. Crommie, Giant bandgap renormalization and excitonic effects in a monolayer transition metal dichalcogenide semiconductor, Nat. Mater. **13**, 1091 (2014).

[46] J. Zhang, Z. Peng, A. Soni, Y. Zhao, Y. Xiong, B. Peng, J. Wang, M. S. Dresselhaus, and Q. Xiong, Raman spectroscopy of few-quintuple layer topological insulator Bi_2Se_3 nanoplatelets, Nano Lett. **11**, 2407 (2011).

[47] W. Dang, H. Peng, H. Li, P. Wang, and Z. Liu, Epitaxial heterostructures of ultrathin topological insulator nanoplate and graphene, Nano Lett. **10**, 2870 (2010).

[48] M. Eddrief, P. Atkinson, V. Etgens, and B. Jusserand, Low-temperature Raman fingerprints for few-quintuple layer topological insulator Bi_2Se_3 films epitaxied on GaAs, Nanotechnology **25**, 245701 (2014).

[49] U. Gupta, B. S. Naidu, U. Maitra, A. Singh, S. N. Shirodkar, U. V. Waghmare, and C. N. R. Rao, Characterization of few-layer 1T-$MoSe_2$ and its superior performance in the visible-light induced hydrogen evolution reaction, APL Mater. **2**, 092802 (2014).

[50] C. Grosse, M. B. Alemayehu, M. Falmbigl, A. Mogilatenko, O. Chiatti, D. C. Johnson, and S. F. Fischer, Superconducting ferecrystals: Turbostratically disordered atomic-scale layered $(PbSe)_{1.14}(NbSe_2)_n$ thin films, Sci. Rep. **6**, 33457 (2016).

[51] See Supplemental Material at http://link.aps.org/supplemental/10.1103/wn8y-xvyh for additional XP spectra, LEED patterns, XRD scans, and AFM analysis.

[52] K. V. Emtsev, F. Speck, T. Seyller, L. Ley, and J. D. Riley, Interaction, growth, and ordering of epitaxial graphene on SiC{0001} surfaces: A comparative photoelectron spectroscopy study, Phys. Rev. B **77**, 155303 (2008).

[53] C. H. Park, B.-H. Cheong, K.-H. Lee, and K. J. Chang, Structural and electronic properties of cubic, 2H, 4H, and 6H SiC, Phys. Rev. B **49**, 4485 (1994).

[54] T. Böker, R. Severin, A. Müller, C. Janowitz, R. Manzke, D. Voß, P. Krüger, A. Mazur, and J. Pollmann, Band structure of Mo_2, $MoSe_2$, and α-$MoTe_2$: Angle-resolved photoelectron spectroscopy and *ab initio* calculations, Phys. Rev. B **64**, 235305 (2001).

[55] V. Boechko and V. Isarev, Crystallization conditions and properties of single crystals of p-type Bi_2Se_3, Izv. Akad. Nauk SSSR, Neorg. Mater. **11**, 1510 (1975).

[56] F. Göhler, Oberflächenphysikalische Untersuchungen an ferekristallinen Dünnschichten und van-der-Waals Heterostrukturen, Ph.D. thesis, Technische Universität Chemnitz, 2022.

[57] G. F. Harrington and J. Santiso, Back-to-basics tutorial: X-ray diffraction of thin films, J. Electroceram. **47**, 141 (2021).

[58] M. Birkholz, *Thin Film Analysis by X-Ray Scattering* (Wiley-VCH, Weinheim, 2006).

[59] D. M. Hamann, D. R. Merrill, S. R. Bauers, G. Mitchson, J. Ditto, S. P. Rudin, and D. C. Johnson, Long-range order in $[(SnSe)_{1.2}]_1[TiSe_2]_1$ prepared from designed precursors, Inorg. Chem. **56**, 3499 (2017).

[60] M. Kruskopf, D. M. Pakdehi, K. Pierz, S. Wundrack, R. Stosch, T. Dziomba, M. Götz, J. Baringhaus, J. Aprojanz, C. Tegenkamp, J. Lidzba, T. Seyller, F. Hohls, F. J. Ahlers, and H. W. Schumacher, Comeback of epitaxial graphene for electronics: Large-area growth of bilayer-free graphene on SiC, 2D Mater. **3**, 041002 (2016).

[61] S. Wang, Y. Rong, Y. Fan, M. Pacios, H. Bhaskaran, K. He, and J. H. Warner, Shape evolution of monolayer MoS_2 crystals grown by chemical vapor deposition, Chem. Mater. **26**, 6371 (2014).

[62] W. A. Abdallah and A. E. Nelson, Characterization of $MoSe_2$(0001) and ion-sputtered $MoSe_2$ by XPS, J. Mater. Sci. **40**, 2679 (2005).

[63] J. Scofield, Hartree-Slater subshell photoionization cross-sections at 1254 and 1487 eV, J. Electron Spectrosc. Relat. Phenom. **8**, 129 (1976).

[64] S. Tanuma, C. J. Powell, and D. R. Penn, Calculations of electron inelastic mean free paths. V. Data for 14 organic compounds over the 50-2000 eV range, Surf. Interface Anal. **21**, 165 (1994).

[65] L. V. Yashina, J. Sánchez-Barriga, M. R. Scholz, A. A. Volykhov, A. P. Sirotina, V. S. Neudachina, M. E. Tamm, A. Varykhalov, D. Marchenko, G. Springholz, G. Bauer, A. Knop-Gericke, and O. Rader, Negligible surface reactivity of topological insulators Bi_2Se_3 and Bi_2Te_3 towards oxygen and water, ACS Nano **7**, 5181 (2013).

[66] O. E. Tereshchenko, K. A. Kokh, V. V. Atuchin, K. N. Romanyuk, S. V. Makarenko, V. A. Golyashov, A. S. Kozhukhov, I. P. Prosvirin, and A. A. Shklyaev, Stability of the (0001) surface of the Bi_2Se_3 topological insulator, JETP Lett. **94**, 465 (2011).

[67] V. A. Golyashov, K. A. Kokh, S. V. Makarenko, K. N. Romanyuk, I. P. Prosvirin, A. V. Kalinkin, O. E. Tereshchenko, A. S. Kozhukhov, D. V. Sheglov, S. V. Eremeev, S. D. Borisova, and E. V. Chulkov, Inertness and degradation of (0001) surface of Bi_2Se_3 topological insulator, J. Appl. Phys. **112**, 113702 (2012).

[68] Y. N. Zhang, Communication: Surface stability and topological surface states of cleaved Bi_2Se_3: First-principles studies, J. Chem. Phys. **143**, 151101 (2015).

[69] P. Tsipas, E. Xenogiannopoulou, S. Kassavetis, D. Tsoutsou, E. Golias, C. Bazioti, G. P. Dimitrakopulos, P. Komninou, H. Liang, M. Caymax, and A. Dimoulas, Observation of surface Dirac cone in high-quality ultrathin epitaxial Bi_2Se_3 topological insulator on AlN(0001) dielectric, ACS Nano **8**, 6614 (2014).

[70] M. T. Edmonds, J. T. Hellerstedt, A. Tadich, A. Schenk, K. M. O'Donnell, J. Tosado, N. P. Butch, P. Syers, J. Paglione, and M. S. Fuhrer, Stability and surface reconstruction of topological insulator Bi_2Se_3 on exposure to atmosphere, J. Phys. Chem. C **118**, 20413 (2014).

[71] J. Buha, R. Gaspari, A. E. Del Rio Castillo, F. Bonaccorso, and L. Manna, Thermal stability and anisotropic sublimation of two-dimensional colloidal Bi_2Te_3 and Bi_2Se_3 nanocrystals, Nano Lett. **16**, 4217 (2016).

[72] M. Ostler, F. Speck, M. Gick, and T. Seyller, Automated preparation of high-quality epitaxial graphene on 6H-SiC(0001), Phy. Status Solidi B **247**, 2924 (2010).